DOI: 10.17725/j.rensit.2024.16.089

Analysis of the intrinsic spin-Hall effect in metals for spintronics problems

Vyacheslav K. Ignatjev, Sergey V. Perchenko, Dmitry A. Stankevich

Volgograd State University, https://volsu.ru/

Volgograd 400062, Russian Federation

E-mail: vkignatjev@yandex.ru, perchenko@volsu.ru, stankevich@volsu.ru

Received September 18, 2023, peer-reviewed September 25, 2023, accepted October 02, 2023, published March 15, 2024.

Abstract: **A method for estimating the transverse spin-Hall resistance for polycrystalline samples of pure metals has been proposed. The spin-Hall effect coefficients for various metals of 3-6 periods, including rare-earth lanthanides, have been calculated. It is shown that the sign of the calculated spin-Hall resistance always coincides with the experimental one. For most of the considered metals the calculation result agrees with the experimental data. It is shown that the agreement of the calculation results with experiment can be significantly improved if the used approximations of strong coupling and effective charge are supplemented by the assumption that the interaction of collectivized conduction electrons in the construction of the self-consistent field can be taken into account by the introduction of the effective mass of the conduction electron in the Hamiltonian of the spin-orbit interaction. The reasons for the deviation for aluminum, copper, dysprosium, holmium, and gadolinium are discussed.**

Keywords: **spintronics, spin-Hall effect, spin-orbit interaction, strong coupling approximation, nearest-neighbor approximation, ideal Fermi-gas approximation, self-consistent field, effective charge**

PACS: 67.57.Lm, 72.25.Ba, 75.76.+j

Acknowledgments: The research was carried out of the funds of the Russian Science Foundation grant № 22-22-20035 (https://rscf.ru/en/project/22-22-20035/), as well as the funds of the Volgograd region budget resources.

For citation: Vyacheslav K. Ignatjev, Sergey V. Perchenko, Dmitry A. Stankevich. Analysis of the intrinsic spin-Hall effect in metals for spintronics problems. *RENSIT: Radioelectronics. Nanosystems. Information Technologies,* 2024, 16(1):89-100e. DOI: 10.17725/j.rensit.2024.16.089.

Contents

1. INTRODUCTION

A promising direction for the development of a new generation of information technology and sensor devices [1] is non-magnetic spintronics based on the spin-Hall effect (SHE). It is accepted to distinguish between extrinsic and intrinsic SHE. The main role in the extrinsic SHE, predicted by M.I. Dyakonov and V.I. Perel in 1971 [2], the spin-dependent scattering of conduction electrons on impurity fields plays a major role. Such scattering provides a fraction of spin-polarized current of the order of fractions of a percent with a coherence length of the

order of tens of nanometers. This is sufficient for studies of spin effects in nanostructures, but not for information and biotechnology. The intrinsic SHE predicted by S. Murakami in 2003, J. Sinova in 2004 [3] and soon discovered experimentally [4] occurs due to the spin-orbit interaction of the Rashba-Dresselhaus type [5]. This interaction is caused by the field of atomic nuclei and can be induced by the non-zero orbital momentum of the conduction electron, or directly by its momentum [6].

The intrinsic SHE is that the charge current in pure nonmagnetic metals with strong spin-orbit interaction leads to a measurable transverse spin current [7]. There is also an opposite phenomenon, the inverse spin-Hall effect (ISHE), in that a spin current in a metal creates a transverse charge current [8]. Thus, the intrinsic SHE can be used in spintronics devices for both generation and detection of spin current. It has been experimentally found that in some cases polycrystalline samples exhibit an increase in the angle of the SHE, the fraction of spin-polarized current, and the coherence length compared to single-crystal samples [9].

At present, reliable experimental data on the spin-Hall effect in metals are available. Therefore, within the approximations used in [10], the spin-Hall effect coefficients of nonmagnetic metals of the 5th and 6th periods were calculated [11]. For platinum, tantalum, gold, alpha-tungsten, palladium, molybdenum, and niobium, the calculation of the transverse spin-Hall resistance gave results that agree with the published experimental ones within the measurement error. For beta-tungsten, the calculated values are about 2 times larger than the experimental values, reflecting the anomalously high SHE. The purposeful search for promising materials for spintronics devices, justification of methods for their design, calculation, and optimization of their signal characteristics implies expanding the basis for comparing calculated values with experimental ones. For this purpose, we calculated the constants of the spin-Hall effect for metals of the 4th and 3rd periods, as well as lanthanides.

2. SELF-CONSISTENT FIELD APPROXIMATION FOR COLLECTIVE ELECTRONS

The spin-orbit addition to the energy of a single electron located in a given electric field with potential $\Phi(\mathbf{r})$ has the form [12]

$$\hat{V} = -\frac{\hbar e}{2m^2c^2}\varepsilon_{\alpha\beta\gamma}\hat{s}_\alpha\frac{\partial\Phi}{\partial r_\beta}\hat{p}_\gamma. \quad (1)$$

Here m is the mass of an electron with charge $-e$, $\hbar$ is the reduced Planck constant, c is the speed of light in vacuum, $\varepsilon_{\alpha\beta\gamma}$ is the unit antisymmetric Levi-Civita tensor.

A pure metal crystal can be considered as a homonuclear molecule with metallic bonding. In the framework of the Hartree-Fock one-electron approximation, each collective electron is in a self-consistent field created by ion cores and other collective electrons [13]. The self-consistent field is usually obtained by the method of successive approximations. In the initial approximation, the wave function of a collective electron is considered as a molecular orbital and is represented as a linear combination of atomic orbitals (LCAO approximation).

For any spin state of an electron it is possible to choose such a direction of the z-axis that the projection of its spin on this axis has a certain value s_z, i.e. $\psi(\mathbf{r},\sigma) = \psi(\mathbf{r})\delta(\sigma, s_z)$. In the strong coupling approximation, such a combination for the coordinate part of the wave function can be the Wannier function [14]:

$$\psi(\mathbf{r}) = \frac{1}{\sqrt{N}}\sum_{n=1}^{N}\Psi(\mathbf{r}-\mathbf{R}_n)\exp(i\mathbf{k}\mathbf{R}_n), \quad (2)$$

Here $\Psi(\mathbf{r})$ is the atomic function of the outer electron, $\mathbf{R}_n$ is the translation vector, and N is the number of nodes in the crystallite.

As a model potential of the initial approximation we take the crystal field potential of ion cores with effective charge Ze and coordinates $\mathbf{R}_k$

$$\Phi(\mathbf{r}) = \frac{eZ}{4\pi\varepsilon_0}\sum_{k=1}^{N}\frac{1}{|\mathbf{r}-\mathbf{R}_k|}. \quad (3)$$

Here ε_0 is the electric constant.

If the atomic wave function $\Psi(\mathbf{r})$ in relation (2) is to be considered hydrogen-like as an initial approximation, the value of Z can be estimated by equating the coordinate of the maximum $\rho_{\max}$ of the radial component of this function to the atomic radius R_a.

$$Z = \frac{\rho_{\max} a_B}{R_a},$$

where $a_B = 5.3 \cdot 10^{-10}$ m is the Bohr radius. **Fig. 1** shows an example for estimating the value of Z for a metal of the fourth period, i.e., when the square of the modulus of the radial wave function R_{40} has four maxima.

The approximation of the effective charge in the model potential (3) together with the strong coupling approximation (2) means that, when constructing the self-consistent field for the collective electron, only its interaction with the nuclei and localized electrons of ion cores is taken into account. In the next approximation, the interaction, including exchange, of the collective electron with other conduction electrons should be taken into account. Such interaction is usually taken into account in the analysis of transport phenomena in the framework of the effective mass method. Formally, it is possible to replace in formula (1) the mass of the free electron by the effective mass. However, there is no reason to believe that this should be the effective mass determining the conductivity and thermal conductivity of the metal.

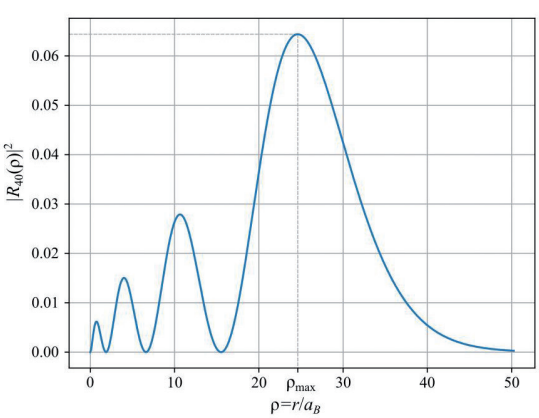

Fig. 1. *Dependence of the square of the absolute value of the radial wave function* $|R_{40}|^2$ *on the dimensionless coordinate* ρ. *Here the principal quantum number n = 4, orbital quantum number l = 0.*

3. DYNAMICS OF THE CONDUCTION ELECTRON MOMENTUM IN A CRYSTAL

Let us consider a mesoscopically homogeneous and isotropic metal. Individual crystallites exhibit anisotropic properties at the microscopic level, but a physically small volume containing a large number of randomly orientated crystallites will not have any distinguished direction. Under mesoscopic homogeneity and isotropy it is meant that there is no regular texture in the sample, i.e. the crystallites are oriented uniformly randomly. Regular texture may be formed during fabrication of the sample, such as mechanical rolling or other deformation of the sample, but not during sputtering. We will also assume that all crystallites have no intrinsic magnetic moment and there are no domain walls, so there is no significant spin perturbation during conduction electron transport across the boundary between crystallites.

The dynamics of the electron momentum created by the perturbation (1) is described by the equation for the mean [13]

$$\frac{dp_\delta}{dt} = \frac{i}{\hbar}\left\langle\left[\hat{V}, \hat{p}_\delta\right]\right\rangle = \\ = \frac{\hbar e \varepsilon_{\alpha\beta\gamma}}{2m^2c^2}\left\langle\psi\left|\hat{s}_\alpha \frac{\partial^2\Phi}{\partial r_\beta \partial r_\delta}\hat{p}_\gamma\right|\psi\right\rangle. \quad (4)$$

Integration over the coordinates and summation over the spin variables of the conduction electron are implied in the right-hand side of relation (4). For any spin state of the electron it is possible to choose such a direction of the z-axis that the projection of its spin on this axis has a certain value s_z, i.e. $\psi(\mathbf{r},\sigma) = \psi(\mathbf{r})\delta(\sigma,s_z)$. Then after summation in (4) on spin variables, putting $\langle\hat{\mathbf{s}}\rangle = \mathbf{s}$ and substituting variables $\mathbf{r} - \mathbf{R}_k \to \mathbf{r}$, we obtain

$$\frac{dp_\delta}{dt} = \frac{\hbar^2 e^2 Z s_\alpha}{8\pi\varepsilon_0 m^2 c^2 N}\sum_{n,m,k=1}^{N}\exp\left(i\mathbf{k}\left(\mathbf{R}_n - \mathbf{R}_m\right)\right)\times \\ \times\left\langle\Psi\left(\mathbf{r}+\mathbf{R}_k-\mathbf{R}_m\right)\left|3\frac{r_\delta}{r^5}\hat{l}_\alpha - \frac{\varepsilon_{\alpha\delta\gamma}}{\hbar r^3}\hat{p}_\gamma\right|\Psi\left(\mathbf{r}+\mathbf{R}_k-\mathbf{R}_n\right)\right\rangle. \quad (5)$$

The operator $3\frac{r_\delta}{r^5}\hat{l}_\alpha - \frac{\varepsilon_{\alpha\delta\gamma}}{\hbar r^3}\hat{p}_\gamma$, in the right-hand side of relation (5) is odd. Therefore, when $\mathbf{R}_n$

$-\mathbf{R}_k = 0$ and $\mathbf{R}_m - \mathbf{R}_k = 0$, its mean value is zero. The atomic functions are exponentially small at $r > R_a = na_B/Z$, n is the principal quantum number. At the same time, the distance between atoms in the crystal is significantly larger than R_a. Therefore, in relation (5) we can restrict ourselves to the nearest-neighbor approximation and leave in the right-hand side only the summands for which $\mathbf{R}_n - \mathbf{R}_k = \mathbf{a}_\nu$ and $\mathbf{R}_m - \mathbf{R}_k = 0$ or $\mathbf{R}_n - \mathbf{R}_k = 0$ and $\mathbf{R}_m - \mathbf{R}_k = \mathbf{a}_\nu$, where $\mathbf{a}_\nu$ is the vector drawn from the atom under consideration with the centre in the point $\mathbf{r} = 0$ to the nearest neighbor. Then, taking into account the Hermiticity of operator in relation (5), we obtain

$$\frac{dp_\delta}{dt} = -\frac{\hbar^2 e^2 Z s_\alpha}{4\pi\varepsilon_0 m^2 c^2}\sin(\mathbf{k}\mathbf{a}_\nu)\times \\ \times \mathrm{Im}\left\langle \Psi_\nu \left| 3\frac{r_\delta}{r^5}\hat{l}_\alpha - \frac{\varepsilon_{\alpha\delta\gamma}}{\hbar r^3}\hat{p}_\gamma \right| \Psi \right\rangle. \quad (6)$$

Here $\Psi_\nu(\mathbf{r}) = \Psi(\mathbf{r} + \mathbf{a}_\nu) - \Psi(\mathbf{r} - \mathbf{a}_\nu)$ is a function with parity opposite to the parity of the function $\Psi(\mathbf{r})$ and the summation by ν over pairs of symmetrically located with respect to the considered atom its nearest neighbors is implied.

The right part of relation (6) is equal to the force acting on the electron. It can be represented as the result of the action of the external electric field $\mathbf{E}_{SH}$ on the electron. In the first order of smallness by $\mathbf{k}\mathbf{a}_\nu$ we obtain:

$$E_{SH\alpha} = \frac{\hbar^2 Z e s_\beta k_\mu}{4\pi\varepsilon_0 m^2 c^2} a_{\nu\mu}\times \\ \times \mathrm{Im}\left\langle \Psi_\nu \left| 3\frac{r_\alpha}{r^5}\hat{l}_\beta - \frac{\varepsilon_{\alpha\beta\gamma}}{\hbar r^3}\hat{p}_\gamma \right| \Psi \right\rangle. \quad (7)$$

Note that the quantum mean in formula (7) splits into two summands, the first of which is proportional to the orbital momentum of the conduction electron and the second to its momentum, which agrees with the models [6].

4. INTRINSIC SPIN-HALL EFFECT IN POLYCRYSTALLINE METAL

Let us consider a macroscopic region of a polycrystalline metal. For any state of an electron it is possible to choose the direction of the quantization axis (z-axis) so that the projection of its orbital momentum on this axis has a certain value $l_z = l$. The energy of an electron in an atom in an electric field depends on the projection of its orbital momentum to the field direction [13]. Therefore, the orientation of the atomic orbitals is determined by the position of the crystallophysical axes of a crystallite and we can consider that the relation (7) is written in the coordinate system associated with the symmetry axes of the crystallite.

Let us introduce a laboratory coordinate system associated with the instruments that set the conduction current and measure the spin components. Therefore, the wave vector and spin vector of conduction electrons should be considered as given in the laboratory coordinate system. The components of the vectors and tensors in the laboratory system will be denoted by primed indices, and in the coordinate system associated with the crystal axes of the domain, not primed.

We transform the wave vector and spin vector of conduction electrons from the laboratory system into the system of crystal axes $k_\mu = p_{\mu\mu'}k_{\mu'}$, $s_\beta = p_{\beta\beta'}s_{\beta'}$, and the vector of the Hall electric field from the system of crystal axes into the laboratory system $E_{SH\alpha'} = p^{-1}_{\alpha'\alpha}E_{SH\alpha}$, where $p_{\alpha'\alpha}$ is a unitary rotation matrix. Substituting this transformation into equation (7), we average the $\mathbf{E}_{SH}$ vector in the macroscopic region over random orientations of crystallites. It is convenient to express the rotation matrix in terms of Euler angles:

$$p_{ij} = \begin{bmatrix} \cos(\alpha)\cos(\gamma) - \sin(\alpha)\cos(\beta)\sin(\gamma) & -\cos(\alpha)\sin(\gamma) - \sin(\alpha)\cos(\beta)\cos(\gamma) & \sin(\alpha)\sin(\beta) \\ \sin(\alpha)\cos(\gamma) + \cos(\alpha)\cos(\beta)\sin(\gamma) & -\sin(\alpha)\sin(\gamma) + \cos(\alpha)\cos(\beta)\cos(\gamma) & -\cos(\alpha)\sin(\beta) \\ \sin(\beta)\sin(\gamma) & \sin(\beta)\cos(\gamma) & \cos(\beta) \end{bmatrix},$$

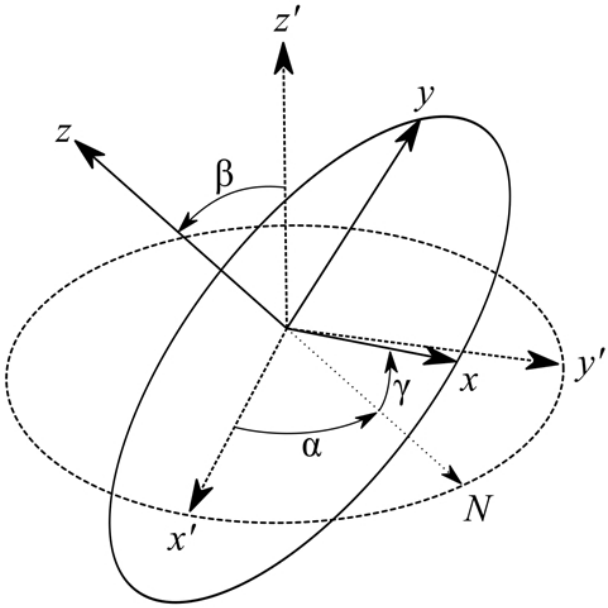

Fig. 2. *Transformation of vector components at transition from the laboratory coordinate system (primed indices) to the system of crystal axes. Here a, β and γ are Euler angles.*

Here $0 \le \alpha \le 2\pi$ is the precession angle, $0 \le \beta \le \pi$ is the nutation angle, $0 \le \gamma \le 2\pi$ is the angle of intrinsic rotation (**Fig. 2**). Then, for a mesoscopically isotropic metal, averaging over random crystallite orientations reduces to averaging over random uniformly distributed Euler angles.

$$E_{SH\alpha'} = \frac{\hbar^2 Zes_{\beta'} k_{\mu'} \overline{p^{-1}_{\alpha'\alpha} p_{\beta\beta'} p_{\mu\mu'}}}{4\pi\varepsilon_0 m^2 c^2} a_{\nu\mu} \times$$
$$\times \mathrm{Im}\left\langle \Psi_\nu \left| 3\frac{r_\alpha}{r^5}\hat{l}_\beta - \frac{\varepsilon_{\alpha\beta\gamma}}{\hbar r^3}\hat{p}_{\gamma\beta} \right| \Psi \right\rangle. \quad (8)$$

Here

$$\overline{p} = \frac{1}{8\pi^2}\int_0^{2\pi}\int_0^{\pi}\int_0^{2\pi} \sin(\beta) p(\alpha,\beta,\gamma)\, d\alpha\, d\beta\, d\gamma. \quad (9)$$

In the analytical averaging of equation (8), integrals of the form (9) were calculated in coordinate form, and then the result was converted to invariant form.

Considering the SHE only in metals, we will use the ideal Fermi-gas approximation for conduction electrons. The applicability of this model for conduction electrons in metals is justified by the fact that the thermodynamics of the Fermi system is determined by its microscopic structure only near the Fermi surface and does not depend at all on what is done beyond a blurring in an energy range of order $k_B T$, where k_B is the Boltzmann constant, T is the temperature.

As a result, the denser the Fermi-gas in a metal, the more ideal it is [15]. Experimental studies of the temperature dependence of the electron heat capacity in metals show that it corresponds well to the model of an ideal Fermi-gas with a scalar effective mass m^*. For many metals $m^* \approx m$. However, for gallium $m^* \approx 2.5m$ and for lanthanum $m^* \approx 0.23m$. Assuming within the effective mass method in (8) $\mathbf{k} = \mathbf{j}m^*/(\hbar e n_e)$, where j is the charge current density, n_e is the concentration of conduction electrons, we obtain

$$\mathbf{E}_{SH} = R_S\left[\mathbf{j}\times\frac{\mathbf{P}}{n_e}\right],$$
$$R_S = \frac{\hbar eZ}{48\pi\varepsilon_0 mc^2}\frac{m^*/m}{en_e}\times \quad (10)$$
$$\times \mathrm{Re}\left\langle \Psi_\nu \left| \frac{3\mathbf{r}(\mathbf{r}\mathbf{a}_\nu) - \mathbf{a}_\nu r^2}{r^5}\frac{\partial}{\partial\mathbf{r}} \right| \Psi \right\rangle.$$

Here $\mathbf{P} = 2\mathbf{s}n_e$ is the spin polarization density vector.

5. CALCULATION OF SPIN-HALL RESISTANCE

The first relation (10) coincides in form with the expression for the electronic Hall effect if we replace the vector $\mathbf{P}/n_e$ by the vector of magnetic induction $\mathbf{B}$. Therefore, it can be expected that the spin-Hall effect constant R_S depends as much on the effective mass of conduction electrons, including its sign, and their concentration as the electronic Hall effect constant $R_H = (m^*/m)/(en_e)$. Then the second part of formula (10) can be written as

$$R_S = \frac{\hbar eZR_H}{48\pi\varepsilon_0 mc^2}\mathrm{Re}\left\langle \Psi_\nu \left| \frac{3\mathbf{r}(\mathbf{r}\mathbf{a}_\nu) - \mathbf{a}_\nu r^2}{r^5}\frac{\partial}{\partial\mathbf{r}} \right| \Psi \right\rangle. \quad (11)$$

The crystal field potential of the form (3) is not centrally symmetric, and the orbital moment of the electron is not a "good" quantum number for it. Therefore, the wave function of an electron in the crystal is different from the wave function of an electron in an isolated atom. Accordingly, the wave function $\Psi(\mathbf{r})$ in relation (2) is not the wave function of an external electron, such as the *s*-electron, of an isolated atom. But it can always be represented as a linear combination of the wave functions of an isolated atom. As a result, in metals the conduction bands overlap, and part of the conduction electrons can be formed by collectivization of *p*-electrons.

Let us use in relation (9) the approximation of hydrogen-like atomic orbital for outer (valence) electrons

$$\Psi_{nlm}(x,\theta,\varphi) = R_{nl}(x)Y_{lm}(\theta,\varphi). \quad (12)$$

Here l is the orbital quantum number, m is the magnetic quantum number, θ is the polar angle, φ is the azimuthal angle, $R_{nl}(x)$ is the radial part of the wave function, $x = Zr/a_B$, $Y_{lm}(\theta, \varphi)$ is the angular wave function (spherical function). The radial hydrogen-like wave function (12) has the form [13]

$$R_{nl}(x) = -\frac{2}{n^2}\sqrt{\frac{(n-l-1)!}{\left[(n+l)!\right]^3}}\times$$

$$\times\exp\left(-\frac{x}{n}\right)\left(\frac{2x}{n}\right)^l L_{n+l}^{2l+1}\left(\frac{2x}{n}\right),$$

Here $L_{n+l}^{2l+1}(t)$ is a generalized Laguerre polynomial. For the *s*-electron, the normalized spherical function is $Y_{00}(\theta,\varphi) = 1/\sqrt{4\pi}$. The normalized spherical function of the p-electron oriented along the polar axis is $Y_{10}(\theta,\varphi) = i\sqrt{3/(4\pi)}\cos(\theta)$.

Let us divide the nearest neighbors of the considered atom into groups with equal distances from it $|\mathbf{a}_\nu| = a_l$, where l = 1, 2, ... is the number of the group of nearest neighbors.

For the *s*-electron of conduction, directing the polar axis along the vector $\mathbf{a}_\nu$, we obtain in each of the nearest neighbor groups

$$\left\langle\Psi_\nu\left|\frac{3\mathbf{r}(\mathbf{r}\mathbf{a}_\nu) - \mathbf{a}_\nu r^2}{r^5}\frac{\partial}{\partial\mathbf{r}}\right|\Psi\right\rangle =$$

$$= m_l\frac{4b_lZ^3}{a_B^3}\int_0^\infty\frac{dR_{n0}(x)/dx}{x}dx\times \quad (13)$$

$$\times\int_0^1 y\left\{R_{n0}(x_1) - R_{n0}(x_2)\right\}dy,$$

Here y = cosθ, $x_1 = \sqrt{x^2 + b_l^2 + 2xb_ly}$, $x_2 = \sqrt{x^2 + b_l^2 - 2xb_ly}$, $b_\nu = Z|a_l|/a_B$, m_1 is the number of pairs of symmetrically located nodes in the *l*-th group of nearest neighbors.

For the *p*-electron of conduction, let us direct the polar axis along the vector $\mathbf{a}_\nu$ and count the azimuthal angle φ from the plane $\mathbf{a}_\nu\mathbf{r}$. In spherical coordinates, $\frac{\partial}{\partial\mathbf{r}} = \frac{\partial}{\partial r}\mathbf{e}_r + \frac{1}{r}\frac{\partial}{\partial\theta}\mathbf{e}_\theta + \frac{1}{r\sin(\theta)}\frac{\partial}{\partial\varphi}\mathbf{e}_\varphi$, with the orth $\mathbf{e}_\varphi$ orthogonal to the plane $\mathbf{a}_\nu\mathbf{r}$ and the orth $\mathbf{e}_\theta$ forming an angle $\pi/2 + \theta$ with the polar axis. Then for the *l*-th group of nearest neighbors we obtain

$$\left\langle\Psi_\nu\left|\frac{3\mathbf{r}(\mathbf{r}\mathbf{a}_\nu) - \mathbf{a}_\nu r^2}{r^5}\frac{\partial}{\partial\mathbf{r}}\right|\Psi\right\rangle =$$

$$= \frac{3b_lZ^3}{2\pi a_B^3}m_l\int_0^\infty\left(\frac{2ydR_{n1}(x)/dx}{x} - \frac{1-y^2}{x^2}R_{n1}(x)\right)dx\times \quad (14)$$

$$\times\int_0^1 y\left\{R_{n1}(x_1) - R_{n1}(x_2)\right\}dy.$$

6. COMPARISON OF CALCULATION RESULTS WITH EXPERIMENTAL VALUES

Table 1 lists the properties of the atoms of the studied metals, the configurations of their electron shells, and the parameters of their crystal lattices.

The spin-Hall effect has been most thoroughly investigated in platinum [16]. For platinum, the atom radius is 139 pm, which for the 6s shell corresponds to $Z \approx 22.45$. The face-centered lattice constant is a = 392 pm, there are 4 atoms per unit cell, and each atom

Table 1

Lattice parameters and electronic configurations of metals

Metal	Lattice	Electronic configuration	r$_a$, pm	Z	a, pm	Pairs of nearest neighbors					
						a_1, пм	m_1	a_2, пм	m_2	a_3, пм	m_3
Au	f.c.c.	[Xe]4f^{14}5d^{10}6s^1	144	21.7	408	288	6	408	3	500	12
Pt	f.c.c.	[Xe]4f^{14}5d^{9}6s^1	139	22.45	392	277	6	392	3	480	12
α-W	b.c.c.	[Xe]4f^{14}5d^{4}6s^2	141	22.77	316	274	4	316	3	449	6
β-W	A15	[Xe]4f^{14}5d^{9}6s^2	141	22.77	504	281	6	436	4	454	6
						251	1	281	1	308	4
Ta	b.c.c.	[Xe]4f^{14}5d^{3}6s^2	147	21	331	286	4	331	3	468	6
Lu	h.c.p.	[Xe]4f^{11}5d^{1}6s^2	175	17.84	351	346	6	492	2	557	1
Ho	h.c.p.	[Xe]4f^{11}6s^2	179	17.44	358	350	6	499	2	562	1
Dy	h.c.p.	[Xe]4f^{10}6s^2	180	17.44	359	353	6	502	2	565	1
Cd	h.c.p.	[Xe]4f^{7}5d6s^{21}	179	17.44	363	359	6	510	2	579	1
Ag	f.c.c.	[Kr]4d105s1	144	14.66	409	289	6	409	3	500	12
Pd	f.c.c.	[Kr]4d105s1	137	15.4	389	275	6	389	3	476	12
Mo	b.c.c.	[Kr]4d105s1	140	15.22	315	273	4	315	3	445	6
Nb	b.c.c.	[Kr]4d105s1	147	14.4	331	287	4	331	3	468	6
Cu	f.c.c.	[Ar]3d104s1	128	10.1	362	256	6	361	3	442	12
α-Mn	A12	[Ar]3d104s1	137	10.25	889	277	8	451	12	460	8
Cr	b.c.c.	[Ar]3d104s1	129	10	289	250	4	289	3	408	6
V	b.c.c.	[Ar]3d104s1	135	9.72	302	262	4	302	3	428	6
Ti	h.c.p.	[Ar]3d104s1	147	8.86	295	291	6	412	2	468	1
Al	f.c.c.	[Ne]3s23p1	143	4.81	495	286	6	405	3	496	12

has 6 pairs of nearest neighbors at a distance of 277 pm, next 3 pairs at a distance of 392 pm and 12 pairs at a distance of 480 pm, b_1 = 117, b_2 = 166, b_3 = 204. At 80 K parameter $R_H = -2\cdot10^{-11}$ m^3/(A·s), for the *s*-electron by formulas (11) and (13) we obtain $R_S = 3.48\cdot10^{-9}$ Ω·m, for the *p*-electron by formulas (11) and (14) we obtain $R_S = -5.12\cdot10^{-10}$ Ω·m.

Table 2 lists the theoretical, calculated by formulas (11), (13) and (14), and experimental values of spin-Hall resistance R_S for different metals. The values of the Hall constant R_H are taken from the reference book [17]. The values of conductivity are taken from the works cited, if they are not given there – from the reference book [17].

In experiment, the spin-Hall angle $\theta_{SH} = \sigma R_S$ is usually determined [9,18,19]. Here σ usually denoted as σ_{xx} is the conductivity of the metal in the absence of spin-orbit interaction. For platinum at 10 K, $\sigma = 8.1\cdot10^6$ Ω^{-1}m^{-1}, $\theta_{SH} = 0.021 \pm 0.005$ [20]. Accordingly $R_S = (2.6 \pm 0.7)\cdot10^{-9}$ Ω·m. Agreement with experiment for *s*-electrons is obtained if in formula (1)

Table 2

Experimental values of spin-Hall effect constants R_S^e and calculated values according to formula (11) R_S^s and R_S^p together with (13) for *s*-electrons and (14) for *p*-electrons.

Metal	σ, 10^5 (Ω·m)$^{-1}$	θ_{SH}, %	R_H, 10^{-11}, m^3/(A·s)	R_S^e, 10^{-9}·Ω·m	R_S^s, 10^{-9}·Ω·m	R_S^p, 10^{-9}·Ω·m
Au	200	0.25±0.05	-7.3	12±3	7.1	-1.08
Pt	81	2.1±0.5	-2	2.6±0.7	3.48	-0.512
α-W	47.6	≈7	11.1	-14.7	-13.96	2.56
β-W	20.4	-35±4	-162	740±80	1660	-294
Ta	3	-0.37±0.1	9.75	-13±4	-15.38	-2.15
Lu	12	1.4±0.2	-12	11±2	9.17	-1.28
Ho	11	14±2	-32	122±17	25.6	-3.34
Dy	18	5±1	-25	28±6	18.0	-2.47
Gd	7	4±1	-12	56±14	6.98	-1.07
Ag	150	0.7±0.1	-8.98	0.47±0.07	-11.7	1.43
Pd	40	0.64±0.1	-8.45	1.6±0.3	-13.4	1.64
Mo	28	-0.8±0.18	18	-2.8±0.7	25.4	-4.41
Nb	11	-0.87±0.2	8.88	-7.9±2	10.1	-11.9
Cu	160	0.32±0.03	-5.36	0.2±0.02	8.32	-1.18
α-Mn	1.42	-0.19±0.01	8.44	-13.3±1	-11.1	1.85
V	55	-1±0.1	7.9	-1.8±0.3	-9.73	1.39
Cr	1.2	-5.1±0.5	36.3	-42±4	-59	8.12
Ti	3.33	-0.036±0.004	1.0	-1.2±0.1	-1.0	0.134
Al	160	0.02±0.01	-3.3	-0.012±0.006	-1.68	0.19

the mass of a free electron is replaced by the effective mass $m^* \approx (1.15 \pm 0.15)m$.

Gold is the second representative of the 6th period and a noble metal. The spin-Hall angle for gold is an order of magnitude smaller than for platinum [21]. The face-centered cubic lattice constant $a = 407.8$ pm, there are 4 atoms per unit cell, 6 pairs of nearest neighbors at a distance of 288 pm, next 3 pairs at a distance of 408 pm and 12 pairs at a distance of 500 pm. Agreement with experiment for *s*-electrons is obtained at $m^* \approx (0.77 \pm 0.1)m$.

Tantalum has a body-centered cubic lattice with constant $a = 331$ pm. There are 2 atoms per unit cell, 4 pairs of nearest neighbors at 286 pm, then 3 pairs at 331 pm and 6 pairs at 468 pm. Agreement with experiment for *s*-electrons will be obtained at $m^* \approx (1.1 \pm 0.1)m$.

Tungsten in the stable alpha-modification has a body-centered cubic lattice with constant $a = 316$ pm. There are 2 atoms per unit cell, 4 pairs of nearest neighbors at 274 pm, then 3 pairs at 316 pm and 6 pairs at 449 pm. In the experiment [22], a value of $|\theta_{SH}| < 0.07$ was obtained on a 15 nm thick film, which corresponds to $|R_S| < 1.47 \cdot 10^{-8}$ Ω·m. The error of the experimentally measured spin-Hall angle in [22] is not given, but the calculated value agrees with the experimental one for *s*-electrons at $m^* \approx (1.0 \pm 0.03)m$.

Tungsten in metastable beta-modification has a lattice of the form A15 for compound AB_3 with constant $a = 503.6$ pm, there are 8 atoms per unit cell. For atom A (in the center and at the corners) there are 6 pairs of nearest neighbors at a distance of 281 pm, then 4 pairs at a distance of 436 pm, 6 pairs at a distance of 454 pm, 3 pairs at a distance of 504 pm, 12 pairs at a distance of 577 pm. For atom B (on the face) 1 pair of nearest neighbors at a distance of 251 pm, then 1 pair at a distance of 281 pm, 4 pairs at a distance of 308 pm, 2 pairs at a distance of 454 pm, 8 pairs at a distance of 471 pm. The calculation shows that atoms A and B contribute equally to the spin-Hall effect. Agreement with the experiment [23, 24] for *s*-electrons is obtained at $m^* \approx (1.5 \pm 0.1)m$.

There are no reliable experimental data on the spin-Hall angle for rare-earth metals. In [25] the value $\xi_{SH} = T_{int}\theta_{SH}$ is given, where T_{int} is the spin transfer coefficient. For estimation we take it equal to 1.

For gadolinium, hexagonal close-packed lattice constants are $a = 363.4$ pm and $c = 578.5$ pm there are 2 atoms per unit cell, 6 pairs of nearest neighbors at 359 pm, then 2 pairs at 510 pm and 1 pair at 579 pm. Agreement with experiment for *s*-electrons will be obtained at $m^* \approx (0.35 \pm 0.05)m$.

For dysprosium, hexagonal close-packed lattice constants are $a = 359.3$ pm and $c = 565.4$ pm there are 2 atoms per unit cell, 6 pairs of nearest neighbors at 353 pm, then 2 pairs at 502 pm and 1 pair at 565 pm. Agreement with experiment for *s*-electrons will be obtained at $m^* \approx (0.8 \pm 0.1)m$.

For holmium, hexagonal close-packed lattice constants are $a = 357.7$ pm and $c = 561.6$ pm there are 2 atoms per unit cell, 6 pairs of nearest neighbors at 350 pm, then 2 pairs at 499 pm and 1 pair at 562 pm. Agreement with experiment for *s*-electrons is obtained at $m^* \approx (0.46 \pm 0.04)m$.

For lutetium, hexagonal close-packed lattice constants are $a = 351$ pm and $c = 556.7$ pm there are 2 atoms per unit cell, 6 pairs of nearest neighbors at 346 pm, then 2 pairs at 492 pm and 1 pair at 557 pm. Agreement with experiment for *s*-electrons will be obtained at $m^* \approx (1.1 \pm 0.1)m$.

Note that of the considered rare-earth metals only lutetium is paramagnetic at all temperatures. At low temperatures dysprosium and holmium are ferromagnets. The magnetic behavior of gadolinium is complex, various magnetic anomalies are

detected [26]. It can be hypothesized that at room temperature they lack only long-range spin ordering but, unlike lutetium, near-order remains. Formula (2) does not take into account the exchange interaction of collective conduction electron with localized magnetization electrons. Therefore, relation (11) applies only to paramagnets such as lutetium. In the presence of near spin ordering, in addition to the spin-Hall electric field of the form (7), there may be a Hall electric field due to the anomalous Hall effect [27]. This phenomenon probably takes place in dysprosium, holmium and gadolinium.

When analyzing the elements of the 5th period, the calculation by formulas (11) and (13) for the *s*-electrons of conduction gives values that do not agree with the experimental ones. This is especially true, apparently, for palladium, which has no 5*s*-electrons.

For silver, the face-centered cubic lattice constant is a = 408.6 pm, there are 4 atoms per unit cell, 6 pairs of nearest neighbors at 289 pm, then 3 pairs at 409 pm, and 12 pairs at 500 pm. Agreement with the experiment [28] for *p*-electrons will be obtained at $m^* \approx (1.75 \pm 0.07)m$.

For molybdenum, the body-centered cubic lattice constant is a = 315 pm, there are 2 atoms per unit cell, 4 pairs of nearest neighbors at 273 pm, then 3 pairs at 315 pm, and 6 pairs at 445 pm. Agreement with the experiment [20] for *p*-electrons will be obtained at $m^* \approx (1.25 \pm 0.15)m$.

For palladium, the face-centered cubic lattice constant is a = 389 pm, there are 4 atoms per unit cell, 6 pairs of nearest neighbors at 275 pm, then 3 pairs at 389 pm, and 12 pairs at 476 pm. Agreement with the experiment [25] for *p*-electrons will be obtained at $m^* \approx (1.0 \pm 0.1)m$.

For niobium, the body-centered cubic lattice constant is a = 331 pm, there are 2 atoms per unit cell, 4 pairs of nearest neighbors at 287 pm, then 3 pairs at 331 pm, and 6 pairs at 468 pm. Agreement with the experiment [20] for *p*-electrons will be obtained at $m^* \approx (1.25 \pm 0.15)m$.

For copper, the face-centered cubic lattice constant is a = 361.5 pm, there are 4 atoms per unit cell, 6 pairs of nearest neighbors at 256 pm, then 3 pairs at 362 pm, and 12 pairs at 442 pm. Agreement with the experiment [29] for *s*-electrons will be obtained at $m^* \approx (6.4 \pm 0.4)m$.

For titanium, hexagonal close-packed lattice constants are a = 295 pm, c = 469.7 pm, there are 2 atoms per unit cell, 6 pairs of nearest neighbors at a distance of 291 pm, then 2 pairs at a distance of 412 pm and 1 pair at a distance of 468 pm. Manganese in alpha modification has structure A12, cubic lattice constant is a = 889 pm, there are 58 atoms per unit cell, 8 pairs of nearest neighbors at a distance of 277 pm, then 12 pairs at a distance of 451 pm and 8 pairs at a distance of 460 pm. Agreement with the experiment [30] for *s*-electrons in titanium and manganese will be obtained at $m^* \approx (0.91 \pm 0.05)m$.

For vanadium, the cubic body-centered lattice constant is a = 302.4 pm, there are 2 atoms per unit cell, 4 pairs of nearest neighbors at a distance of 262 pm, then 3 pairs at a distance of 302.4 pm and 6 pairs at a distance of 427.7 pm. Agreement with the experiment [27] for *s*-electrons will be obtained at $m^* \approx (2.3 \pm 0.2)m$.

For chromium, the cubic body-centered lattice constant is a = 288.5 pm, there are 2 atoms per unit cell, 4 pairs of nearest neighbors at a distance of 249.8 pm, then 3 pairs at a distance of 288.5 pm, and 6 pairs at a distance of 408 pm. Agreement with the experiment

[27] for *s*-electrons will be obtained at $m^* \approx (1.18 \pm 0.05)m$.

For aluminum, the face-centered cubic lattice constant is $a = 405$ pm, there are 4 atoms per unit cell, 6 pairs of nearest neighbors at 286 pm, then 3 pairs at 405 pm, and 12 pairs at 496 pm. Agreement with the experiment [31] for *p*-electrons will be obtained at $m^* \approx (3.9 \pm 1)m$. Aluminum has no *d*- and *f*-electrons on the inner shells. These electrons have a good shielding ability, so for transition and rare-earth metals the use of a hydrogen-like orbital (12) with a corresponding effective charge for the conduction electrons is a justified approximation. For aluminum, such an approximation is apparently inapplicable. In addition, of all the metals considered, only aluminum has a filled *p*-shell. As a result, the contribution to the SHE from *s*- and *p*-electrons almost compensates each other, and the small experimental value of the spin-Hall effect constant R_S is obtained as a difference of two relatively large values, not because of the large effective mass of the charge carriers.

For copper, the experimental value of the spin-Hall effect constant is very small, and as in the case of aluminum, is probably obtained as the difference of two relatively large values. Good agreement with the experiment for copper is obtained if we assume that 90% of the conduction electrons are collective electrons *p*-electrons and 10% are *s*-electrons.

Comparative analysis of the data listed in Tables 1 and 2 shows that for elements of even periods (6th and 4th) the sign of the measured spin-Hall resistance always coincides with the sign calculated for the *s*-electron, and for elements of odd periods (5th and 3rd) – with the sign calculated for the *p*-electron.

7. CONCLUSION

The justification of methods for designing spintronics systems, calculating and optimizing their characteristics requires additional assumptions about the system. Such assumptions are the representation of the wave function of a collective conduction electron as a Wannier function, the effective charge approximation and the nearest-neighbor approximation in the Hamiltonian (5), and the ideal Fermi-gas model for conduction electrons. The applicability of these models for a particular problem should be substantiated experimentally. The intrinsic SHE coefficients calculated within the framework of these models agree with the measured ones. The question of the admissibility of introducing the effective mass of the conduction electron into the spin-orbit interaction Hamiltonian (1) to account for the interaction of collective conduction electrons when constructing the self-consistent field potential (3) in the framework of the one-electron approximation requires further study.

Spin polarization according to the mechanism described in this work does not require external magnetic fields and residual magnetization and therefore does not interfere with work in micro- and nano-sized spintronics structures. Of undoubted interest is the search for new promising materials for spintronics devices based on metal alloys and intermetallic compounds. The design of such spintronics systems, calculation and optimization of their characteristics is possible on the basis of the described methods and approaches, if we consider the crystallite of intermetallic compound as a heteronuclear macromolecule. The methods of constructing molecular orbitals for such structures, including those in the form of Wannier functions, are well studied [32,33].

REFERENCES

1. Bukharaev AA, Zvezdin AK, Pyatakov AP, Fetisov YK. Straintronics: a new trend in micro- and nanoelectronics and materials science. *Phys.-Usp.*, 2018, 61:1175-1212; doi: 10.3367/UFNe.2018.01.038279.
2. Dyakonov MI, Perel VI. Current-induced spin orientation of electrons in semiconductors. *Physics Letters A*, 1971, 35(6):459-460; doi: 10.1016/0375-9601(71)90196-4.
3. Sinova J, Culcer D, Niu Q, Sinitsyn NA, Jungwirth T, MacDonald AH. Universal Intrinsic Spin Hall Effect. *Phys. Rev. Lett.,* 2004, 92(12):126603-126606; doi: 10.1103/PhysRevLett.92.
4. Wunderlich J, Kaestner B, Sinova J, Jungwirth T. Experimental observation of the spin-Hall effect in a two dimensional spin-orbit coupled semiconductor system. *Phys. Rev. Lett.*, 2005, 94(4):047204-047216; doi: 10.1103/PhysRevLett. 94.047204.
5. Zhang S. Spin torques due to large Rashba fields. In book "*Spin Current*", Edited by Maekawa S, Valenzuela SO, Saitoh E, Kimura T. Oxford, University Press, 2012, pp 424–431.
6. Sinova J, Valenzuela SO, Wunderlich J, Back CH, Jungwirth T. Spin Hall effects. *Reviews of Modern Physics,* 2015, 87:1213-1259; doi: 10.1103/RevModPhys.87.1213.
7. Hoffmann A. Spin hall effects in metals. *IEEE Transactions on Magnetics,* 2013, 49(10):5172-5193; doi: 10.1109/TMAG.2013.2262947.
8. Saitoh E, Ueda M, Miyajima H, Tatara G. Conversion of spin current into charge current at room temperature: Inverse spin-Hall effect. *Applied Physics Letters*, 2006, 88:182509; doi: 10.1063/1.2199473.
9. Xiao Y, Wang H, Fullerton EE. Crystalline Orientation–Dependent Spin Hall Effect in Epitaxial Platinum. *Frontiers in Physics*, 2022, 9:791736; doi: 10.3389/fphy.2021.791736.
10. Ignatjev VK, Lebedev NG, Stankevich DA. The effect of the spin polarization control of conduction electrons through the deformation of a ferromagnet. *Technical Physics Letters,* 2022, 48(12):25-28; doi: 10.21883/TPL.2022.12.54941.19363,
11. Ignatjev VK, Lebedev NG, Stankevich DA. The spin Hall effect in polycrystalline samples of nonmagnetic fifth- and sixth-period metals. *Technical Physics Letters,* 2023, 49(3):60-62; doi: 10.21883/TPL.2023.03.55688.19437.
12. Berestetskii VB, Pitaevskii LP, Lifshitz EM. *Teoreticheskaya fizika. T. IV. Kvantovaya electrodinamika* [Course of Theoretical Physics, Vol. 4, Quantum Electrodynamics]. Moscow, Fizmatlit Publ., 2002, 720 p.
13. Landau LD, Lifshitz EM. *Teoreticheskaya fizika. T. III. Kvantovaya mehanika. Nerelyativ-istskaya teoriya* [Course of Theoretical Physics, Vol. 3, Quantum Mechanics. Non-relativistic Theory]. Moscow, Fizmatlit Publ., 2004, 800 p.
14. Madelung O. *Teoiriya tverdogo tela* [Theory of solid states]. Moscow, Nauka Publ., 1980, 416 p.
15. Kvasnikov IA. *Teoriya ravnovesnyh sistem: Statisticheskaya fizika* [Theory of equilibrium systems: Statistical physics]. Moscow, Editorial URSS, 2002, 240 p.
16. Sinova J, Valenzuela SO, Wunderlich J, Back CH, Jungwirth T. Spin Hall effects. *Reviews of Modern Physics,* 2015, 87:1213; doi: 10.1103/RevModPhys.87.1213.
17. Cardarelli F. *Materials Handbook*. Springer International Publishing AG. Switzerland. 2018.
18. Dyakonov MI, Khaetskii AV. Spin Hall effect. In book "*Spin Physics in Semiconductors*". Edited by Dyakonov MI. Chapter 8, Ser. in Solid-State Sciences. New

York, Springer, 2008, 157:211-243; doi: 10.1007/978-3-319-65436-2_8.
19. Dyakonov MI. Magnetoresistance due to edge spin accumulation. *Physical Review Letters,* 2007, 99(12):126601; doi: 10.1103/PhysRevLett.99.126601.
20. Morota M, Niimi Y, Ohnishi K, Wei DH, Tanaka T, Kontani H, Kimura T, Otani Y. Indication of intrinsic spin Hall effect in 4d and 5d transition metals. *Physical Review B*, 2011, 83:74405; doi: 10.1103/PhysRevB.83.174405.
21. Vlaminck V, Pearson JE, Bader SD, Hoffmann A. Dependence of spin pumping spin Hall effect measurements on layer thickness and stacking order. *Physical Review B*, 2013, 88(6):064414; doi: 10.1103/PhysRevB.88.064414.
22. Pai C-F, Liu L, Tseng HW, Ralph DC, Buhrman RA. Spin transfer torque devices utilizing the giant spin Hall effect of tungsten. *Applied Physics Letters*, 2012, 101(12):122404- 122412; doi: 10.1063/1.4753947.
23. Hao Q, Chen W, Xiao G. Beta (β) tungsten thin films: Structure, electron transport, and giant spin Hall effect. *Applied Physics Letters*, 2015, 106(18):182403; doi: 10.1063/1.4919867.
24. Hao Q, Xiao G. Giant Spin Hall Effect and Switching Induced by Spin-Transfer Torque in a W/Co40Fe40B20/MgO Structure with Perpendicular Magnetic Anisotropy. *Physical Review Applied,* 2015, 3:034009; doi: 10.1103/PhysRevApplied.3.034009.
25. Reynolds N, Jadaun P, Heron JT, Jermain CL, Gibbons J, Collette R, Buhrman RA. Schlom DG, Ralph DC. Spin-Hall Torques Generated by Rare-Earth (Lanthanide) Thin Films. *Physical Review B*, 2017, 95:064412; doi: 10.1103/PhysRevB.95.064412.
26. Belov KP, Belyanchikova MA, Levitin RZ, Nikitin SA. *Redkozemel'nye ferromagnetiki i antiferromagnetiki* [Rare-earth ferromagnets and antiferromagnets]. Moscow, Nauka Publ., 1965, 320 p.
27. Smejkal L, MacDonald AH, Sinova J, Nakatsuji S, Jungwirth T. Anomalous Hall antiferromagnets. *Nature Reviews Materials,* 2022, 7:482-496, doi: 10.1038/s41578-022-00430-3.
28. Wang HL, Du CH, Pu Y, Adur R, Hammel PC, Yang FY. Scaling of Spin Hall Angle in 3d, 4d, and 5d Metals from Y3Fe5O12. Metal Spin Pumping. *Physical Review Letters,* 2014, 112: 197201, doi: 10.1103/PhysRevLett.112.197201.
29. Mosendz O, Vlaminck V, Pearson JE, Fradin FY. Bauer GEW, Bader SD, Hoffmann A. Detection and quantification of inverse spin Hall effect from spin pumping in permalloy/normal metal bilayers. *Physical Review B*, 2010, 82(21):214403, doi: 10.1103/PhysRevB.82.214403.
30. Du C, Wang H, Yang F, Hammel C. Systematic variation of spin-orbit coupling with d-orbital filling: Large inverse spin hall effect in 3d transition metals. *Physical Review B*, 2014, 90:40407, doi: 10.1103/PhysRevB.90.140407.
31. Valenzuela S, Tinkham M. Direct electronic measurement of the spin Hall effect. *Nature,* 2006, 442:176-179; doi: 10.1038/nature04937.
32. Bazilevskij MV. *Metod molekulyarnyh orbit i reakcionnaya sposobnost' organicheskih molekul* [Molecular orbital method and reactivity of organic molecules]. Moscow, Himiya Publ., 1969, 304 p.
33. Gribov LA, Mushtakova SP. *Kvantovaya himiya* [Quantum chemistry]. Moscow, Gardariki Publ., 1999, 390 p.